5.8-GHz FMCW Radar System for Drone Tracking

Jason Merlo, *Student Member, IEEE*, Stavros Vakalis, *Student Member, IEEE*,
Cory Hilton, *Student Member, IEEE*, and Jacob Randall

***Abstract*—The design of a portable frequency-modulated continuous-wave (FMCW) radar system for detecting and localizing drones is discussed in this report. The system utilized the 5.8 GHz industrial, scientific and medical band and occupied a 100 MHz bandwidth. The system is able to localize drones at a range of 10 m or more. The theory behind FMCW radar localization is explained, and an algorithm for detecting the drone response is presented. The design considerations of a radar board and transmit and receive patch antenna arrays are discussed. We include experimental measurements of tracking a drone.**

***Index Terms*—Drone, detection, FMCW radar, localization**

I. Introduction

DRONES, and in general unmanned aerial vehicles, have become increasingly popular as they offer numerous benefits to commercial and research applications. However, these novel advances from using drones do not come without the dangers of potential misuse which can lead to significant privacy issues, safety concerns, and property damage [1].

Radar is an excellent candidate for detecting and tracking drones and it is a mature technology that has been used for tracking aerial objects for decades. It is currently being used in a variety applications including environmental remote sensing [2], vital sign detection [3], imaging [4], and non-destructive testing [5]. Radar systems have a unique advantage in remote sensing as they can provide all-weather, 24/7 monitoring, which optical imagers cannot. This is due to the relatively long wavelength of microwave radiation, which can propagate through fog, clouds, smoke, and some building materials with minimal attenuation. Additionally, radar does not depend on illumination from an external source such as the sun.

As a result, radar drone sensing has become an increasingly popular research area with many different works utilizing continuous-wave (CW), frequency-modulated continuous-wave (FMCW), and interferometric radar [6]–[9]. A large amount of the CW works have focused on detecting the presence of a drone, with many of them focusing on micro-Doppler signatures [10] and classifying them using neural networks [11], however in this work we will focus primarily on localization and tracking of the drone.

II. FMCW Radar for Range-Doppler Mapping

Consider an FMCW radar configuration with a single transmitter and two receivers as shown in Fig. 1. The waveform coming from the transmitter can be written as

$$s(t) = \cos\left[2\pi\left(f_0 t + \tfrac{K}{2}t^2\right)\right] \tag{1}$$

The authors are with the Department of Electrical and Computer Engineering, Michigan State University, East Lansing, MI 48824 USA (e-mail: merlojas@msu.edu; vakaliss@msu.edu; hiltonc2@msu.edu).

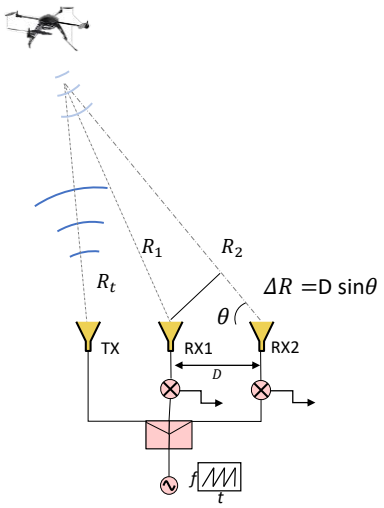

Fig. 1. DoA estimation using an FMCW radar with a single transmitter and two receivers.

where f_0 is the starting frequency of the chirp, and $K = \beta/\tau$ is the chirp rate where β is the bandwidth of the chirp and τ is the duration of the chirp. The normalized received signals at the output of the mixers after propagating in free space and reflecting off of a drone as shown in Fig. 1 can be written as

$$v_1(t) = \cos\left[2\pi(K\frac{R_t + R_1}{c}t)\right] \tag{2}$$

$$v_2(t) = \cos\left[2\pi(K\frac{R_t + R_2}{c}t)\right] \tag{3}$$

where R_t is the distance from the transmitter to the drone and R_i is the distance from the drone to the ith receiver. A Fourier transform (FT) can be used to compute the instantaneous frequencies of $v_1(t)$, $v_2(t)$. Because the transmitters and receivers are separated by a small distance compared to the distance from the array to the drone, it can be assumed that $R_t \approx R_i$. This distance can be shown to be

$$R_i = \frac{f_i c}{2K} \tag{4}$$

where f_i is the instantaneous frequency of the ith receiver. Based on the far-field approximation, the range of the target can be written as $R = \frac{R_1+R_2}{2}$. The angle information can be found from the difference in propagation distance that the wavefront travels between receivers 1 and 2. For direction of arrival (DoA) estimation it can not be assumed that $R_1 \approx R_2$ as this difference is exploited to perform the angle estimation. Based on that,

$$\sin\theta = (R_1 - R_2)/D \tag{5}$$

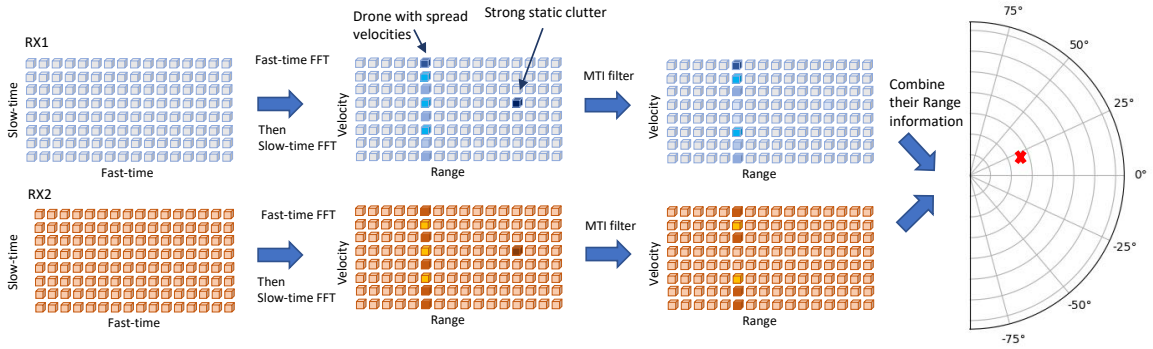

Fig. 2. Range-Doppler map and DoA signal processing chain. In the received matrices on the left, the cubes represent samples from the DAQ. After the FT produces the range-Doppler maps in the two center frames, the cubes represent power spectral density at each range and velocity. A polar plot of the target location is depicted on the right which is formed from the frequency content in the range-Doppler maps.

where θ is the residing angle of the drone relative to the broadside of the array and D is the baseline between the two receive antennas. Thus, using (2) and (3) it can be shown that

$$\theta = \sin^{-1}\left[\frac{(f_1 - f_2)c}{KD}\right]. \tag{6}$$

Velocity estimation can also be implemented using an FMCW radar. In this work, we will use the velocity information from the received signal to determine if there is a drone in the scene and perform localization only on the drone reflections and ignore the surrounding clutter. The velocity estimation can be performed over multiple pulses by observing subtle variations in phase over equiphase points over successive chirp spectra. This can be performed via a FT, along the slow-time dimension, which refers to time samples between different pulses of the waveform. Range estimation, on the other hand, takes place on the fast-time dimension, which refers to time samples in the same pulse period. The velocity ν of a moving target can be found through the angular frequency ω along the slow-time dimension,

$$\nu = \frac{\lambda\omega}{4\pi T} \tag{7}$$

where λ is the center wavelength and T is the pulse repetition period.

III. Signal Processing Algorithm

A visualization of the signal processing algorithm used in this system can be seen in Fig. 2. For every receiver we capture the responses of M pulses and we create a 2-D matrix. The horizontal dimension of the matrix represents the fast-time and the vertical dimension of the matrix represents the slow-time. By performing an FT along the fast-time dimension and applying (4), each pulse can be converted into a range estimate. In order to estimate the velocity we perform a second FT along the slow-time dimension and apply (7). The result of these two FTs is the Range-Doppler map. It is shown in Fig. 2 that the Range-Doppler maps produced by each of the two receivers contains a drone and a static clutter at a stronger amplitude than the drone. Due to the fast rotation of the blades on the drone, large Doppler spread is induced at the drone's location; this can be seen in the response of the drone that is spread on the velocity axis. On the other hand, the stationary clutter shows only a strong peak with zero velocity.

It is desirable to remove the clutter as it could be mistaken for a drone based on its high relative return strength; to do this a moving target indication filter is utilized. This can be implemented by using a notch filter in the velocity axis centered at $\nu = 0$, or by simply setting the power spectral density of the zero-Doppler column equal to a zero vector if the bins are sufficiently wide. Afterwards, to differentiate the drone from the rest of the clutter, the range corresponding to the maximum mean-square response as a function of time was found. If the mean-square velocity value is above a threshold value, the response will be considered as coming from a drone. Finally, the ranges from the two receivers will be used to perform angle estimation as in (6). Once both the range and angle of the drone are estimated, the drone can be localized in a 2-D plane as a function of downrange and crossrange in meters.

Although this report focuses on only detecting and tracking a single drone, this algorithm can be easily adapted to track multiple drones due to the fact that different drones will typically have different range and velocity profiles. Based on the uniqueness of these quantities, the individual responses may be isolated in the receivers' Range-Doppler map and afterwards be used to perform localization easily and effectively.

IV. System Hardware

A. Radar Design

The radar system was designed to use a single transmitter and up to four receivers. The radar system schematic and a subsystem overview from a layout perspective can be found in Figs. 3 and 4 respectively. A photograph of the fully assembled radar board can be seen in Fig. 5. At a high level, the board was functionally divided into the transmitter, receiver, and power subsystems.

1) Subsystems: The transmitter subsystem design revolved around a Texas Instruments LMX2491 6.4 GHz programmable phase-locked loop (PLL) integrated circuit (IC) and ramp generator. The PLL charge pump output was passed through an external active loop filter before entering an Analog Devices

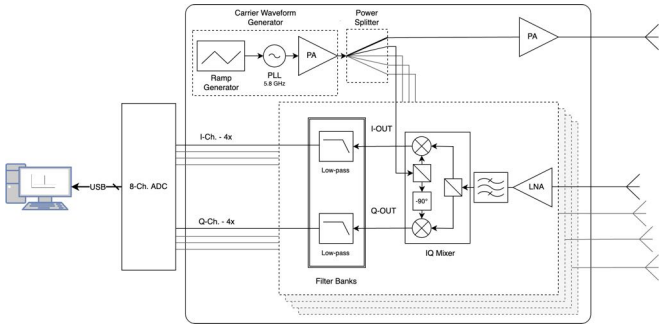

Fig. 3. High level schematic of the radar system.

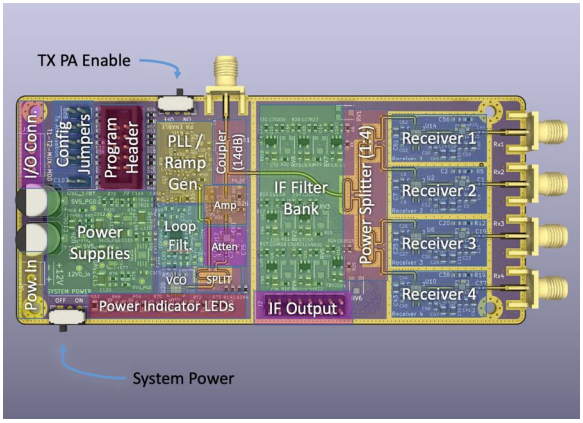

Fig. 4. Annotated render of the radar system with subsystem blocks highlighted.

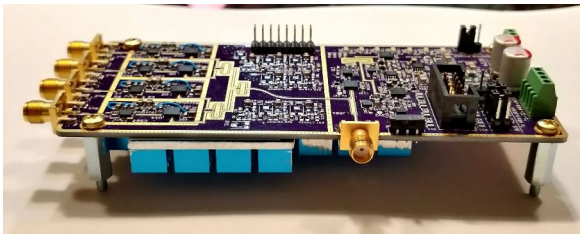

Fig. 5. Photograph of the fully assembled radar board.

(ADI) HMC431 5.5 GHz–6.1 GHz voltage-controlled oscillator. This signal was then split by a 3 dB Wilkinson divider to send half of the signal back to the PLL as feedback and half to a user-selectable variable attenuator prior to be amplified by a Qorvo TQP5523 32 dB power amplifier. Finally, the signal was passed through a 14 dB coupler where $\sim 4\%$ of the power was split to drive the mixers in the receivers and the remainder of the power was sent to the transmit antenna.

The receiver subsystem consisted of four receivers each containing an ADI HMC717A 14.5 dB low-noise amplifier followed by an ADI HMC951A 5.6 GHz–8.6 GHz downconverter. The local oscillator (LO) inputs were driven by the signal siphoned from the final stage of the transmitter; this signal was split four ways through three 3 dB Wilkinson dividers in a 1:4 configuration to drive each downconverter. Once downconverted, the signals were passed through an active intermediate frequency (IF) low-pass filter with a tunable gain of 0–20dB[1]. Finally, the IF signals were sent to a Measurement Computing USB-1608-FS-Plus DAQ where all eight signals were simultaneously and synchronously sampled at 100 kSps and triggered by the start of a new ramp on the transmitter.

To satisfy the power requirements for all devices, voltage levels at 10, 5.5, 5.25, 5.0, 3.3, and 3.0 volts, in addition to a 10.8–13.2 volt power source were required. The 10 V rail utilized a single low-dropout regulator (LDO), however the majority of the ICs required a 5 V input or less; for efficiency, a DC/DC converter was used to step down the input to an intermediate 5.5 V. This voltage was filtered through two LDOs to create 5.25 V and 5.0 V rails. Finally, the 5.0 V rail was used to create 3.3 V and 3.0 V rails using two more LDOs. To further reduce noise in the system, many components used ferrite beads in addition to decoupling capacitors on their power inputs.

2) Physical Requirements: The board for this project was designed to be both low-cost and simple enough to build in a typical lab environment[2]. To allow for high performance radio frequency (RF) integrated circuits to be used, the decision was made to use reflow soldering enabling the use of quad flat no-lead packages as are commonly used in these devices. To maintain ease of assembly, all surface mount devices were confined to a single side of the board which allowed for a single reflow pass without the need for adhesives to hold chips to the bottom side of the board. OshPark was chosen as the printed circuit board (PCB) manufacturer due to their low cost electroless nickel immersion gold plated boards which are well suited for reflow soldering and rework, and availability of 4-layer boards using ISOLA FR408-HR substrate which has favorable RF characteristics ($\epsilon_r = 3.64,\ \tan\delta = 0.0098$) in the 5.8 GHz industrial, scientific and medical band. To keep the PCB designs accessible to the widest audience, the open-source, cross-platofrom, electronic design suite KiCad was used for the schematics, layout, and 3D model of the board.

3) Layout Considerations: The board was separated into three isolated sections based on noise sensitivity. These can be seen isolated by the gold via-fenced sections on the PCB in Fig. 4. The section on the left side of Fig. 4 consists of all the power, digital, and transmitter circuitry as these were deemed to have the highest noise tolerance and also emit the largest amount of noise. The center section contained the IF electronics and 1:4 splitter for the LO inputs of the receivers. Finally, the right, most sensitive, section of the board in Fig. 4 contained the receivers with added fencing between each receiver to avoid coupling between channels.

In addition to via-fencing between subsystems, all microstrip RF transmission lines employed via-fencing around them to increase isolation. Furthermore, via-fencing was added to the edges of the board to reduce radiated RF emissions from the edges of the board. The unused space on the top and bottom signal layers was filled with ground pours and stitched

[1]Due to a biasing issue, the IF filters were bypassed in the final design, however sensitivity was still found to be acceptable for detecting the bulk response from a drone

[2]The board built for this project was assembled in an apartment using standard soldering tools and a modified toaster oven for reflow soldering

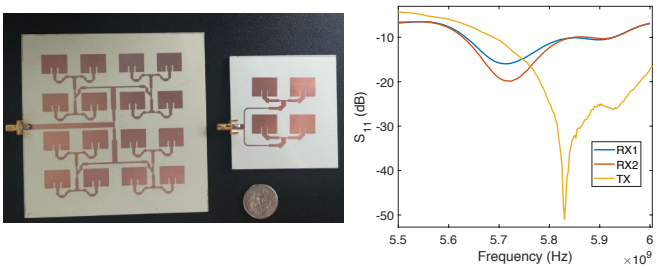

Fig. 6. (left) Photograph of the transmitter 4x4 patch antenna array and the receiver 2x2 patch antenna array. (right) Measured S_{11} parameters for the transmit and two receive patch antennas.

Category	Cost
Circuit Board	$505.30
Manufacturing Supplies	$47.38
Mounting/Fastening	$30.04
Off-board Power	$39.48
Data Acquisition & Programming	$548.32
Cables	$159.60
Total:	**$1,330.12**

Fig. 7. Summary of the bill of materials.

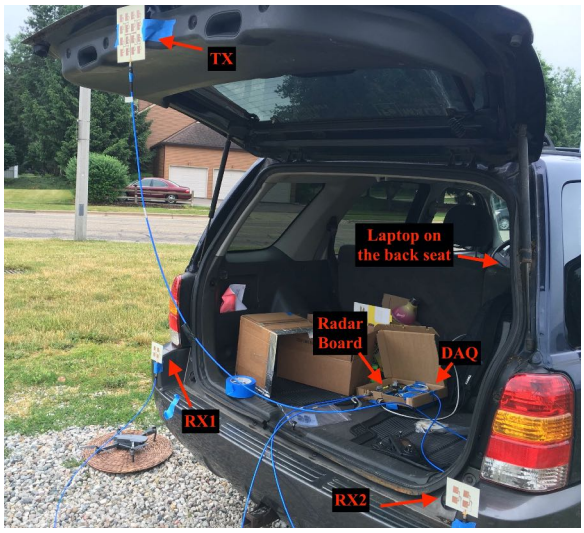

Fig. 8. Photograph of the experimental radar configuration.

together using vias to ensure no unintentional resonators were formed. Finally, solder mask was left off the via-fence areas for the addition of metal RF shieldsif needed.

The board utilized several distributed planar element components, all of which were designed using AutoCAD and simulated in Ansys HFSS. The elements include four 3 dB Wilkinson dividers which were used in the transmitter and receiver LO fan-out, a 14 dB coupler to draw a small signal from the transmitter to drive the receiver LOs, and an SMA transition to minimize reflections while transitioning from the coaxial SMA connector pin to the narrower microstrip line on the PCB. The transition was designed by removing the copper layers directly below the transition to create a coplanar to microstrip transition and then used an optimizer to find the ideal transition length and spacing between the pin and the top layer ground plane to minimize the power loss.

B. Antennas

Patch antenna arrays were designed and simulated in Ansys HFSS. We chose patch antennas arrays due to their simple fabrication process on a PCB. The transmit antenna was a 4x4 array, while the receive antennas were 2x2 arrays to provide an increased field of view for angle estimation. The substrate chosen was Rogers RO4350B with a thickness of $1.524\,\mathrm{mm}$. The antennas were etched on the substrate using a photolithography process. A photograph of the transmit antenna and one of the two receive antennas can be seen on the left of Fig. 6. The measured S_{11} of the three antennas can be seen on the right of Fig. 6.

The antennas were designed using the basic rectangular patch antenna dimension calculations [12] and were then tuned to the desired frequency in HFSS. Using these equations, the patch dimensions were found to be W=16.91 mm and L=12.85 mm. The microstrips for these arrays were calculated using Keysight ADS. The patches were spaced to have a center to center separation distance of 0.95λ to minimize coupling and possible side-lobes that could be later observed. The feedlines for both antennas were created primarily using $50\,\Omega$ to $100\,\Omega$ splits and utilizing quarter-wave transformers to step the transmission line impedance back down to $50\,\Omega$. To account for a minor over-etching during manufacturing, a dilation of 1.5% was applied to the finished design.

C. Bill of Materials

A summary of the bill of materials (BOM) can be found in Fig. 7. A detailed itemized and categorized BOM listing all components and recommended tools can be found at https://docs.google.com/spreadsheets/d/14kPDrza__Lf1kQ5HlxRQW3g6EeMugPi_6xZNXxwF0A4/.

V. Experimental Measurements

Experimental measurements for tracking a drone were run outdoors. The experimental setup can be seen in Fig. 8 in the trunk of a car. The radar PCB along with the DAQ and programmer were placed inside a box. The chirp used for these measurements had a bandwidth of $100\,\mathrm{MHz}$ ranging from $5.775\,\mathrm{GHz}$–$5.875\,\mathrm{GHz}$ with a pulse repetition frequency of $4\,\mathrm{kHz}$. Two receivers were used which separated by a baseline of $1.397\,\mathrm{m}$. The single transmitter was mounted higher from the rest of the system and the antennas to avoid coupling. A laptop was used to implement the signal processing algorithm and real-time visualization. A snapshot of the real-time visualization can be seen in Fig. 9 next to a photograph of the drone flying.Our system manages to track the drone in real-time, and a recording will be included in the presentation video.

VI. Conclusion

In this report, a portable radar system capable of tracking drones was presented. Using two receivers and a single trans-

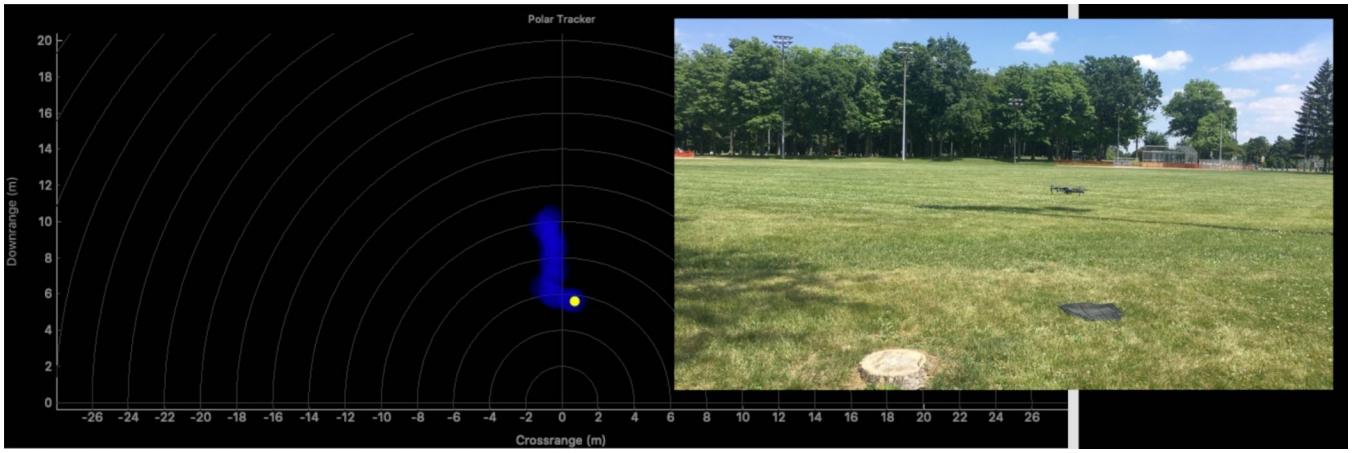

Fig. 9. Real-time visualization of the drone tracking. The yellow dot represents the estimated location of the drone and the blue tail indicates the estimated path previously flown by the drone. The drone was approaching the receiver and slowing down before landing during this screen capture.

mitter we are able to demonstrate the principles of tracking drones up to a range of $\sim 10\,\mathrm{m}$. It has also been shown that the system can be replicated inside a home or university lab and provides many facets of radar systems, antenna, and microwave system design, as well as signal processing that can be used for teaching radar principles.

REFERENCES

[1] R. Altawy and A. M. Youssef, "Security, privacy, and safety aspects of civilian drones: A survey," *ACM Trans. Cyber-Phys. Syst.*, vol. 1, no. 2, Nov. 2016. [Online]. Available: https://doi.org/10.1145/3001836

[2] P. C. Dubois, J. van Zyl, and T. Engman, "Measuring soil moisture with imaging radars," *IEEE Transactions on Geoscience and Remote Sensing*, vol. 33, no. 4, pp. 915–926, 1995.

[3] Y. He, C. Gu, H. Ma, J. Zhu, and G. V. Eleftheriades, "Miniaturized circularly polarized doppler radar for human vital sign detection," *IEEE Transactions on Antennas and Propagation*, vol. 67, no. 11, pp. 7022–7030, 2019.

[4] M. Klemm, J. A. Leendertz, D. Gibbins, I. J. Craddock, A. Preece, and R. Benjamin, "Microwave radar-based differential breast cancer imaging: Imaging in homogeneous breast phantoms and low contrast scenarios," *IEEE Transactions on Antennas and Propagation*, vol. 58, no. 7, pp. 2337–2344, 2010.

[5] A. Boryssenko, O. Boryssenko, A. Lishchenko, and V. Prokhorenko, "Inspection of internal structure of walls by subsurface radar," *IEEE Aerospace and Electronic Systems Magazine*, vol. 21, no. 10, pp. 28–31, 2006.

[6] S. Rahman and D. A. Robertson, "Radar micro-doppler signatures of drones and birds at k-band and w-band," *Sci Rep*, vol. 8, no. 17396, pp. 2–21, 2018.

[7] S. Björklund, "Target detection and classification of small drones by boosting on radar micro-doppler," in *2018 15th European Radar Conference (EuRAD)*, 2018, pp. 182–185.

[8] R. I. A. Harmanny, J. J. M. de Wit, and G. P. Cabic, "Radar micro-doppler feature extraction using the spectrogram and the cepstrogram," in *2014 11th European Radar Conference*, 2014, pp. 165–168.

[9] J. A. Nanzer and V. C. Chen, "Microwave interferometric and doppler radar measurements of a uav," in *2017 IEEE Radar Conference (RadarConf)*, 2017, pp. 1628–1633.

[10] V. C. Chen, F. Li, S. . Ho, and H. Wechsler, "Micro-doppler effect in radar: phenomenon, model, and simulation study," *IEEE Transactions on Aerospace and Electronic Systems*, vol. 42, no. 1, pp. 2–21, 2006.

[11] A. Huizing, M. Heiligers, B. Dekker, J. de Wit, L. Cifola, and R. Harmanny, "Deep learning for classification of mini-uavs using micro-doppler spectrograms in cognitive radar," *IEEE Aerospace and Electronic Systems Magazine*, vol. 34, no. 11, pp. 46–56, 2019.

[12] C. A. Balanis, *Antenna theory: analysis and design*. John wiley & sons, 2016.

Jason Merlo received the B.S degree in computer engineering from Michigan State University in 2018. He is currently a Ph.D. student studying electrical engineering at Michigan State University working in the Electromagnetics Research Group (EMRG). His research interests include distributed radar, interferometric arrays, radar detection and tracking, and radar in robotics, aerospace, and automotive applications.

Stavros Vakalis received the Diploma degree in electrical and computer engineering from National Technical University of Athens, Athens, Greece in 2017, and the M.S. degree in electrical and computer engineering from Michigan State University, East Lansing, MI, USA in 2020. He is currently pursuing his Ph.D. His current research interests include wireless microwave and millimeter-wave systems, millimeter-wave imaging, antenna arrays, radar and signal processing.

Cory Hilton is an electrical engineering senior undergraduate student at Michigan State University. Since 2019, he has been an undergraduate member of the Distributed Electromagnetics Theory and Applications (DELTA) group, where he has been conducting research in harmonic tag design. Cory will seek to continue his education with a Ph.D. at Michigan State University.

Jacob Randall is an electrical engineering senior undergraduate student at Michigan State University. He is part of the Solar Racing Team and has contributed several designs towards the latest multi-occupant vehicle, Aurora. His research experience in the Electromagnetic Research Group, under the supervision of Dr. Nanzer, includes antenna design, interferometric methods, and signal processing of object tracking data.